Appl. Phys. B 73, 85–91 (2001) / Digital Object Identifier (DOI) 10.1007/s003400100613

Applied Physics B
Lasers
and Optics

$CH_4/air/SO_2$ premixed flame spectroscopy with a 7.5-μm diode laser

D. Weidmann*, A. Hamdouni, D. Courtois

Groupe de Spectrométrie Moléculaire et Atmosphérique, UMR CNRS 6089, Université de Reims Champagne-Ardenne, U.F.R. Sciences Exactes et Naturelles, B.P. 1039, 51687 Reims cedex 2, France

Received: 19 February 2001/Revised version: 18 April 2001/Published online: 7 June 2001 –

Abstract. As sulfur dioxide (SO_2) is often involved in combustion processes, we present here SO_2-concentration measurements in the post-flame region of a $CH_4/air/SO_2$ premixed flame. SO_2 concentrations were deduced from high-resolution absorption spectra recorded with a mid-infrared tunable diode-laser (TDL) source operating at liquid nitrogen temperature. Single-mode, continuous frequency tuning around 1384.5 cm^{-1} (or 7.5 μm) is achieved by a fine TDL temperature ramp. These experiments lead us to develop in situ combustion-pollutant measurements with compact apparatus. We show that this non-intrusive method is efficient for detection and allows the retrieval of SO_2 concentration and temperature.

PACS: 42.55.Px; 42.62.Fi; 82.33.Vx

Sulfur dioxide (SO_2) is both a natural pollutant and an anthropogenic product. It has a high toxicity; it easily dissolves in atmospheric water and produces the very harmful phenomenon called acid rain (sulfuric acid). It occurs in nature in volcanic smoke and gases [1], but a wide rate of atmospheric sulfur dioxide is produced near industrial plants. Oil, coal and natural gas often contain sulfur compounds; thus, after combustion, sulfur dioxide is widely present in burned gases.

It is of interest to develop in situ SO_2-concentration measurements, especially in the post-flame region of a burner. These measurements have been achieved by tunable diode-laser spectroscopy, a useful technique to investigate the combustion phenomena whatever the gas we probe [2–4]. The advantage of this method is that measurements are non-intrusive. One can make measurements in high-temperature gas flow. For the mid-infrared SO_2 spectroscopy, the ν_3 band (centered around 1362 cm^{-1}) is well suited because the line strengths are very strong (6×10^{-20} cm^{-1}/molecule cm^{-2}). The working spectral region must be carefully chosen. We present here our laboratory-built burning system and the spectroscopic experimental device. Then experimental records are shown and discussed. Recorded spectra have been fitted to retrieve temperature and SO_2 concentration.

*Corresponding author.
(Fax: +33-0/3-2691-3147, E-mail: damien.weidmann@univ-reims.fr)

1 Spectral region selection

The SO_2 molecule, belonging to the C_{2v} group, has three fundamental vibrational transitions: ν_1 (centered at 1152 cm^{-1}), ν_2 (518 cm^{-1}) and ν_3 (1362 cm^{-1}). The ν_2 vibration is rather difficult to study with diode lasers. We also have to take care of absorption interference by other combustion compounds. Moreover, atmospheric water-vapor absorption must not perturb the measurements.

As shown in Fig. 1, in the mid infrared, it is interesting to work with the ν_3 band of SO_2 according to the transition line strengths. This band is not superimposed with CO_2 and CO bands, which are major combustion products. However, Fig. 1 shows that the $\nu_1 + \nu_2 + \nu_3$ band of CH_4 (1310 cm^{-1}) and the ν_2 band of H_2O (1595 cm^{-1}) can be superimposed with the ν_3 band of SO_2.

Lastly, the most severe feature limiting our choice of working spectral region is the diode laser itself.

2 Experimental details

2.1 Diode laser

The diode-laser source and the tuning protocol have been already described [6]. The lead salt diode laser emitting in the mid infrared has been provided by the Fraunhofer-Institut für Physikalische Meßtechnik. It is a double-heterostructure diode laser [7], which operates around 1380 cm^{-1} at the temperature of 65 K. This temperature is reached by pumping above liquid nitrogen (LN_2) contained in the diode-laser dewar. The injection current is fixed and a fine ramp temperature tuning, 5 K spread at 1 K/min, enables a single-mode emission of five different modes successively. We took care that the emission was single-mode to avoid partition noise [8] and a temperature-tuning protocol allows a continuous frequency change.

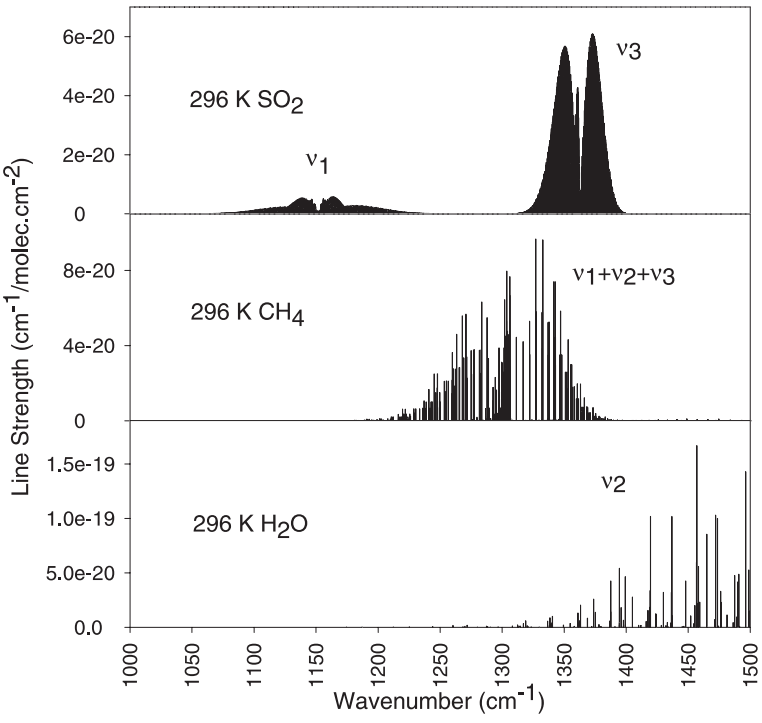

Fig. 1. Spectra of SO_2, CH_4 and H_2O based on Hitran96 [5] data

A diode laser is approximately continuously tunable over the spectral region around $1\,cm^{-1}$. The diode laser used emits between 1380 and $1400\,cm^{-1}$ by mode hopping of $3.5\,cm^{-1}$. By experimentally analyzing the five different emission modes, we kept one mode continuously tunable between 1384.0–$1384.8\,cm^{-1}$. In this spectral range atmospheric water vapor and methane absorption is insignificant. Moreover at these wavelengths high-temperature H_2O absorption lines exist, which will make it possible to deduce the post-flame-region temperature.

2.2 Flat-flame burner design

Reproducible measurements on a combustion system need to use a very steady flame. The laminar premixed low-pressure flat flame is appropriate.

We built our burner in the laboratory on the specifications described in [9]. It is sketched in Fig. 2. The hatched parts are aluminum; blank parts are zones filled with fluids. The burner itself is a 2-cm-diameter sintered stainless steel disk of 43% porosity. The pore diameter is between 12 and 25 μm. The aim of this flame holder is to make the mixture radial speed distribution at the end of the burner tube uniform and, moreover, it avoids flame strike-back. The burner is enclosed in a 6-cm-diameter low-pressure cell. The low-limit operating pressure, depending on burner diameter, is 70 Torr. To operate at lower pressure than this value requires a burner with larger dimensions, since the flame-quenching diameter is inversely proportional to the surrounding pressure [10]. Low-pressure work is achieved by a high flow rate pump; pressure is controlled by a depression manometer. The pumping flow rate is accurately controlled by a needle valve; a safety vacuum buffer is introduced between the burner system and the pump. A cold-water circuit in the burner barrel prevents system and burned gases overheating. The cell uses BaF_2 windows 9.4-cm apart, permitting the laser-radiation probe to go

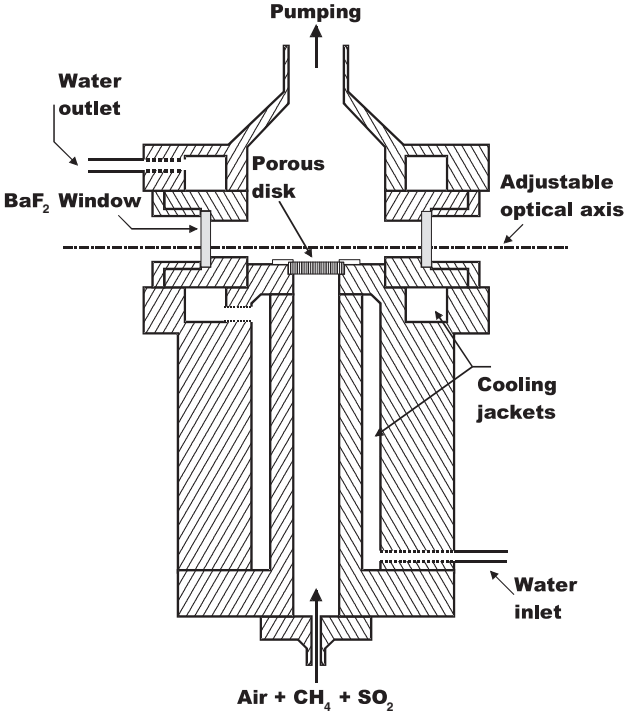

Fig. 2. Low-pressure flat-flame burner

through the cell. The distance between optical axis and burner surface is adjustable by mean of two beam steerers.

Flow meters, equipped with precision valves, were used to control air, methane and sulfur dioxide flows. Then, these three gases were mixed together and injected into the burner tube as shown in Fig. 2. Of course, the tube length is such that the flow is laminar; in our case the Reynolds' number is around 500.

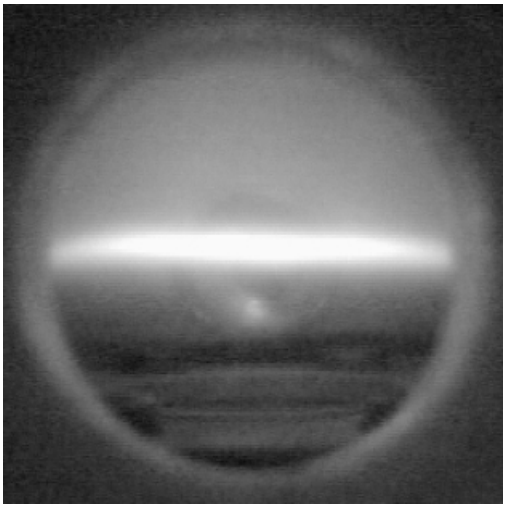

Fig. 3. Typical low-pressure flat flame

Two hermetic feed-throughs were designed on the cell walls. Two movable tungsten needles (1-mm diameter) produce the flame-ignition spark. Once the flame is lit, the needles are moved away from the flame. A movable thermocouple is placed in the other feed-through. The thermocouple position can be adjusted in two directions. The first permits us to measure the temperature versus radial distance to the burner center; the other to measure the temperature versus height to the flame holder.

Figure 3 shows a visible CCD image typical of the obtained flames.

2.3 Optical setup

The experimental setup used for absorption spectroscopy through the burner is shown in Fig. 4. The laser radiation emitted by the diode is collected by a 90°-off-axis parabolic mirror (PM), with a focal length $F = 50$ mm, opened at $F/2$. The beam size is then reduced to 4-mm diameter with a confocal two-lens system. A mechanical chopper (MOD), operating at 2800 Hz, is placed at the focus of the reducing system, where the diode laser is imaged. The reducing system output beam is divided into two parts by a 25%-reflection beam splitter (BS).

The first beam goes through a confocal Fabry–Perot etalon (CFP) designed and built in the laboratory [11]. The mirrors are parallel BaF_2 meniscuses 250-mm apart. The concave meniscus is dielectric-coated and the reflectivity of this coating is 80% at our working wavelength. The convex meniscus is antireflection-coated. After the radiation has passed through the CFP, it is detected by a LN_2-cooled photoconductive HgCdTe detector. The CFP is used as a relative frequency reference; its free spectral range (FSR) is 10^{-2} cm^{-1}. The single-mode emission of the laser is immediately checked by the fringe appearance (Fig. 6).

The other part of the beam goes through the burner cell via two beam steerers. The signal is then measured by a detector similar to the first.

Signals are sent to two lock-in amplifiers with a 3-ms time constant, and recorded by a numerical acquisition system with a 10-ms integration time.

3 Temperature measurements

We will show below that temperature is a key parameter to deduce concentrations from experimental spectra.

At first, we made measurements in the burner cell with a small-diameter (0.2 mm) thermocouple. The thermocouple used is a C (tungsten–5% rhenium/tungsten–26% rhenium) type. Its tolerance is 1% of the measured value. We recorded a radial temperature profile, shown in Fig. 5.

Once results of measurements are corrected for radiative losses [12], the mean temperature 14 mm above the flame front is then 1294 K.

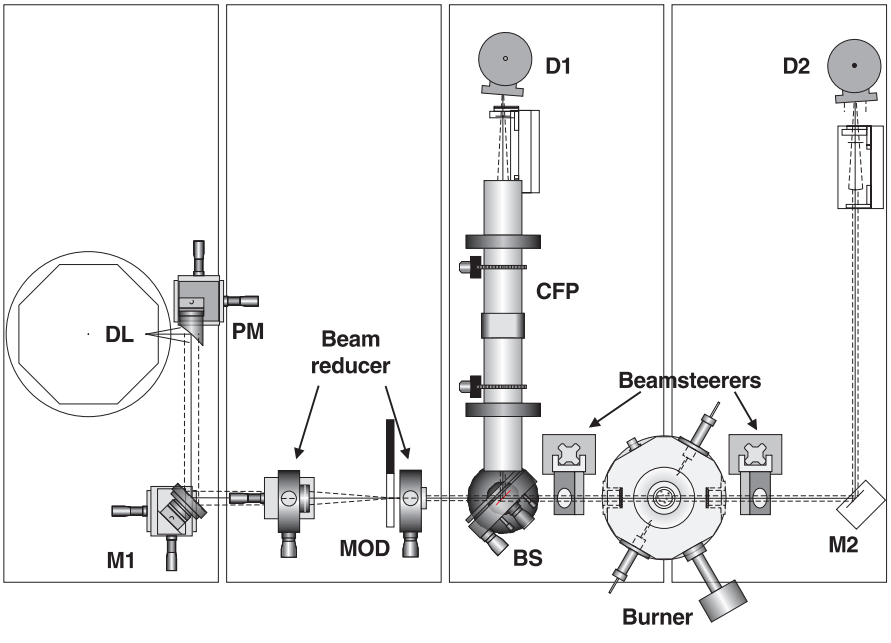

Fig. 4. Experimental optical setup

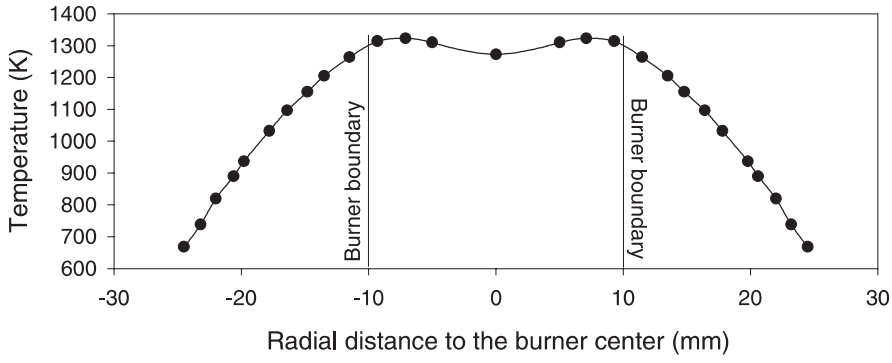

Fig. 5. Radial profile of temperature 14 mm above the burner

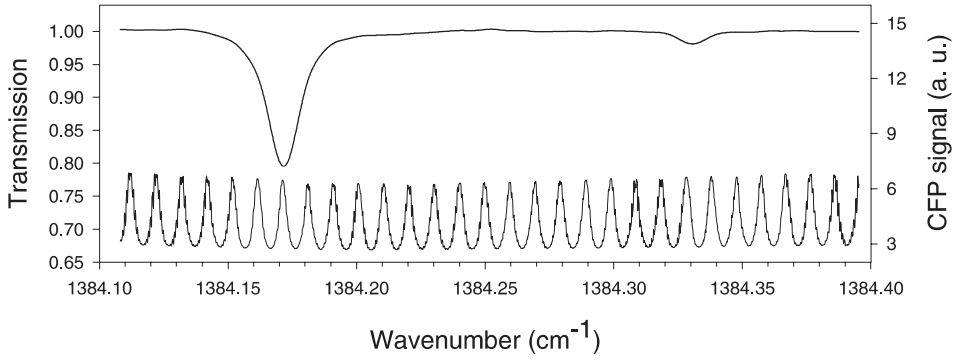

Fig. 6. H_2O spectrum in the post-flame region

The second way for estimating the temperature is based on the temperature-dependence of the line strength of the transition. For a transition i one has

$$S_i(T) = S_i(T_0)\frac{Q(T_0)}{Q(T)}\exp\left[-\frac{hcE_i''}{k}\left(\frac{1}{T}-\frac{1}{T_0}\right)\right] \times\left[1-\exp\left(\frac{hc\sigma_i}{kT}\right)\right]\left[1-\exp\left(-\frac{hc\sigma_i}{kT_0}\right)\right]^{-1}, \quad (1)$$

where $S_i(T)$ is the line strength at temperature T, $S_i(T_0)$ is the known line strength at the temperature reference T_0 (296 K), Q is the rovibrational partition function, h is the Planck constant, c is the speed of light, k is the Boltzmann constant, σ_i is the wavenumber and E_i'' is the lower-state energy of the transition.

If we have a molecular spectrum containing two transitions i and j from different lower states, we can measure the ratio $S_i(T)/S_j(T)$. This ratio depends only on $S_i(T_0)$, $S_j(T_0)$, E_i'', E_j'', T, T_0, σ_i and σ_j. Except for T, these are known parameters available from spectroscopic data compilations. We used Hitemp96, the extension of Hitran96 for high temperature.

We recorded a high-temperature H_2O spectrum in a 102 Torr CH_4/air flame without SO_2 injection. SO_2 is not an active compound of combustion, and its relative concentration is low so the perturbation of the flame temperature is not significant. The spectrum is shown in Fig. 6. It has been frequency-calibrated by using CFP lines. The absolute frequency reference is the strongest line position taken in Hitemp96, and listed in Table 3. Two absorption lines appear with different lower states. Then, after computing the transition line strengths, the temperature is found to be 1210 ± 30 K. The uncertainty on this value has been obtained by taking 10% of total relative uncertainty on the two line strengths calculated from the experimental spectrum.

Taking into account various thermocouple-measurement uncertainties (uncertainties on reference-junction temperature, on measured junction temperature and uncertainty related to thermomaterial inhomogeneities) thermocouple measurements of post-flame region temperature give 1294 ± 30 K. One can note a slight difference between the results obtained by the two previous measuring methods. Two phenomena can explain this shift. Since the flame is not isolated from the surroundings, some water, produced by the combustion reaction, can diffuse and thus perturb the optical measurement. In addition, the probing diode-laser beam is located 4 mm above the flame front (luminous zone). Therefore, in this region, the temperature is not stable yet and still grows at a 40 K/mm rate. The temperature deduced by the two-line method then gives an effective temperature integrated over the beam area. We will see that the difference of 84 K between the two measured values leads to a SO_2-concentration underestimation of 0.32 Torr.

4 Absorption theory and analysis model

Given a homogenous medium of length L_j, the transmittance $\tau(\sigma)$ of laser radiation, at wavenumber σ passing through it is given by Beer's law

$$\tau(\sigma) = \exp\left[-\sum_j \alpha_j(\sigma)L_j\right], \quad (2)$$

where $\alpha_j(\sigma)$ is the absorption coefficient at wavenumber σ, and j is an index of the eventual different media (or cells).

Table 1. Coefficients of the partition function polynomial approximation from Hitran96

Temperature range		70–500 K	500–1500 K
H_2O coefficients	a	–4.440500	–9.432700E+01
	b	0.276780	8.190300E–01
	c	1.253600E–03	7.400500E–05
	d	–4.893800E–07	4.243700E–07
SO_2 coefficients	a	–2.405600E+02	–2.116200E+04
	b	1.110100E+01	1.184600E+02
	c	2.216400E–02	–1.664800E–01
	d	5.233400E–05	1.682500E–04

Then, $\alpha_j(\sigma)$ is given by

$$\alpha_j(\sigma) = \sum_k \sum_i S_{jki}(T_j)\phi_{jki}(\sigma, T_j, P_{jk',jk})P_{jk}\,, \tag{3}$$

where k and k' are indices of the different gases filling the cell j, i is an index of the absorption-line set, T_j is the temperature of the cell j and S_{jki} is the line strength of the ith absorption line from the kth gas occurring in the jth cell. ϕ_{jki} is the normalized line shape of the transition. We used, in our case, an approximation of the Voigt line shape given by Olivero and Longbothum [13]. P_{jk} is the partial pressure of the kth gas in the jth cell. The line strength $S_{jki}(T_j)$ depends on the rovibrational partition function $Q_k(T_j)$. To calculate $Q_k(T_j)$, we used the polynomial approximation of the total internal partition sum temperature dependence coming from Hitran96:

$$Q_k(T_j) = a + bT_j + cT_j^2 + dT_j^3\,. \tag{4}$$

Coefficients a, b, c and d are tabulated in the database for three different temperature ranges. Table 1 presents the coefficients we used.

Molecular concentrations can be derived by fitting a theoretical synthetic spectrum to the experimental one. Updated computational approaches allow us to obtain this parameter through iterative non-linear least-squares calculations. An algorithm, initially developed for atmospheric terrestrial spectra [14], has been modified into a laboratory multi-spectral fitting program [15].

In this work, frequencies and line strengths are kept fixed; their values are taken from Hitran96 and Hitemp96. Temperatures are known from our measurements (see above), and keep fixed too. So the algorithm has been adapted to retrieve the partial pressure in the particular cell that is a burner. At the same time, the program is able to estimate all the different molecular contributions in the burner cell. Moreover, it adjusts the base line and the global frequency calibration of the spectra.

5 Concentration measurements

To calculate the synthetic spectra, we divided the burner cell into three parts (Fig. 7): a first cell of length L_1, the cell 1, where gases are at temperature T_1; a cell 2 of length L_2, which corresponds to the post-flame medium, where gases are at temperature T_2; lastly, a cell 3, which is equivalent to the cell 1.

Of course temperature and concentration edges are not so abrupt. Nevertheless, in this way, one can determine an effective concentration of SO_2 present in the post-flame region.

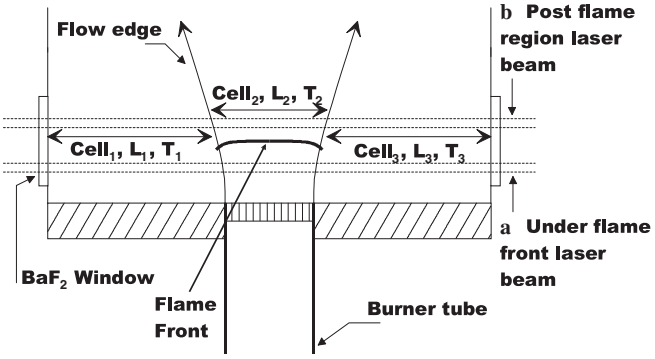

Fig. 7. The burner divided into three cells

According to the flow diffusion leaving the burner tube, L_2 must be greater than the flame-holder diameter (2 cm).

Figure 8a and b show two spectra, one recorded with the laser beam under the flame front (Fig. 8a), the other with the laser beam in the post-flame region, probing high-temperature gases (Fig. 8b). These spectra have been recorded with a burner-cell pressure of 110 Torr. First of all, qualitatively, one can note the effect of high temperature on the second spectrum; both spectra are at the same scale. Indeed, the SO_2 in the post-flame region is at a high temperature and according to the rotational levels occupation, the line strength of the transitions decreases. Indeed, when one compares the Boltzmann rotational levels distributions at 296 K and 1300 K, it appears that for $J'' < 45$ the rotational levels are depleted at 1300 K, and the rotational levels population for $J'' < 45$ is enhanced. That explains the absorption decrease for the spectrum recorded in the post-flame region (see Table 2). Moreover, for this spectrum, an absorption line due to high-temperature water (stemming from the combustion reaction) is present; it corresponds to the strong water line observed in a non-SO_2-doped flame (see Fig. 6 and Table 3). This line vanishes in the spectrum recorded under the flame front, indicating the lack of high-temperature water.

Frequencies and line strengths of the strongest lines appearing in the experimental spectra are listed in Tables 2 and 3.

The analyzed spectrum is the one recorded with the laser beam probing the post-flame region (Fig. 8b). To retrieve SO_2 concentration with our algorithm, we have to fix some of the parameters. We took L_2 equal to 2.5 cm (slightly greater than the flame-holder diameter). This value corresponds to the observed diameter of the flame front with the visible CCD camera. The cell-2 temperature is the result of the two-line method measurement, viz. 1210 K. For the cell-1 and cell-3 lengths, we took the complementary length, viz. 3.45 cm. The temperatures of these cells were taken equal to the surrounding medium mean temperature, 540 K. Thus, the post-flame region SO_2 partial pressure found is 1.51 Torr, which leads to a concentration of 1.3%. According to the accuracy of our flow meters, the SO_2 partial pressure should be 1.6 ± 0.3 Torr. The agreement is correct. The calculated spectrum never differs from the observed one by more than 2%. The global RMS of the residual is 1.4×10^{-4}. With this method using a three-layer model and mean temperatures, we deduced a mean partial pressure. But, the advantage is to avoid intrusive temperature measurements in the flame, which is not so easy. In return, measuring the surrounding mean tem-

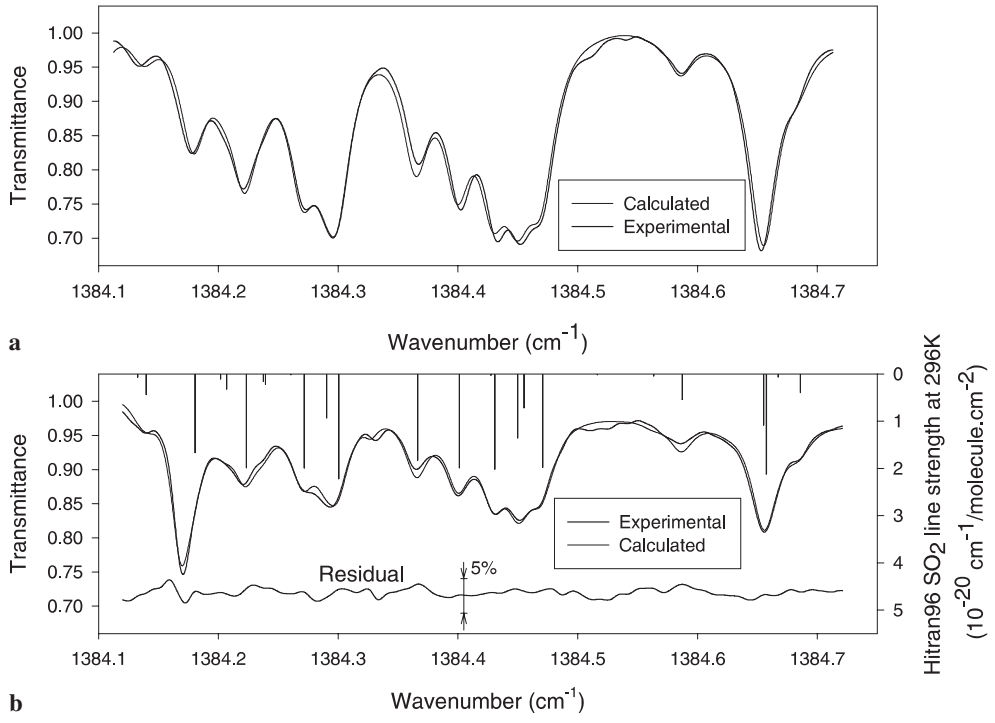

Fig. 8. a SO_2 spectra recorded with beam probing the fresh gases under the flame front, **b** same spectrum, but with beam probing the burned gases in the post-flame region. On the *top axis*, SO_2 line strengths are sketched

Table 2. Hitran96 data for 296 K SO_2 strongest ($> 10^{-21}$ cm^{-1}/molecule cm^{-2}) lines observed on experimental spectra

Frequency (cm^{-1})	Line strength (cm^{-1}/molecule cm^{-2})	Lower-state energy (cm^{-1})	J'' (lower)
1384.13971	4.39E–21	794.7205	41
1384.18057	1.66E–20	512.1743	37
1384.20179	1.08E–21	1093.9195	45
1384.20676	3.18E–21	863.6545	42
1384.22343	1.99E–20	471.5944	36
1384.23751	1.57E–21	1013.2798	44
1384.23929	2.26E–21	936.5161	43
1384.27150	1.99E–20	477.8335	37
1384.29045	9.31E–21	636.7320	39
1384.30049	2.22E–20	450.8016	36
1384.36634	1.83E–20	493.9847	37
1384.40111	1.99E–20	490.2974	39
1384.43068	2.02E–20	492.6180	40
1384.44980	1.36E–20	558.1388	38
1384.45509	7.15E–21	694.3472	40
1384.47073	1.98E–20	484.9207	38
1384.58726	5.38E–21	755.9758	41
1384.65517	1.08E–20	608.1866	39
1384.65742	2.12E–20	460.1980	36
1384.68577	3.96E–21	821.5877	42

Table 3. Hitemp96 data for 1200 K H_2O strongest ($> 4 \times 10^{-22}$ cm^{-1}/molecule cm^{-2}) lines observed on experimental spectra

Frequency (cm^{-1})	Line strength (cm^{-1}/molecule cm^{-2})	Lower-state energy (cm^{-1})	J'' (lower)
1384.16994	8.14E–21	2495.1660	8
1384.32847	4.01E–22	4750.3790	10

perature is convenient. However, this temperature should be determined accurately, since the deduced SO_2 partial pressure depends on temperature according to the quantity

$$\frac{\Delta P_{SO_2}}{\Delta T} = 3.8 \times 10^{-3}\,\text{Torr/K}\,.$$

We checked the results obtained by this simple model by using a more sophisticated one. This time, we took into account the temperature profile measured in the burner cell (Fig. 5). The burner cell was modeled by 16 different layers of known lengths and temperatures, according to our temperature measurements. Concentrations of molecular species were assumed constant in the burner cell. The SO_2 partial pressure retrieved is thus 1.55 Torr. The fit of the calculated spectrum with the observed one is of course enhanced. The global RMS of residual values falls to 0.9×10^{-4}. Agreement with the first fitting procedure is actually valid; the results of our former model are justified.

Lastly, our instrumental signal to noise ratio is around 1000. We took a very strong criterion for deducing the detection limit of SO_2: we considered that we were able to detect an absorption line if the line depth is 10 times as great as the noise level. This means that the detection limit is achieved for a 99% transmittance (or 1% absorbance). If we select the strongest SO_2 absorption line appearing in our spectrum, such a criterion corresponds with a SO_2 partial pressure of 0.1 Torr. With the working conditions here presented (total pressure of 110 Torr), the corresponding concentration is 0.1%.

6 Conclusion

We have presented an approach that leads to the measurement of hot SO_2 concentration in a combustion process. For this purpose, we developed and built a low-pressure flat-flame

burner and fed it with a SO_2-doped oxidant (air) and fuel (CH_4) mixture. This kind of system can be used for fundamental spectroscopy in order to feed a high-temperature database like Hitemp96. Another application is in situ concentration measurements of high-temperature SO_2, which are of environmental interest. With our mid-infrared diode-laser system we measured the flame temperature in a non-intrusive way, and by fitting experimental spectra we retrieved a SO_2-concentration estimation. The system can be useful too as a SO_2 detector, with a detection limit around 0.1%.

Acknowledgements. We would like to thank J. Poncelet and P. Von Der Heyden for their helpful advice and for the burner mechanical realization.

References

1. C. Oppenheimer: Int. J. Remote Sensing **19**, 2829 (1998)
2. S.M. Schoenung, R.K. Hanson: Combust. Sci. Technol. **24**, 227 (1981)
3. B. Rosier, P. Gicquel, D. Henry, A. Coppalle: Appl. Opt. **27**, 360 (1988)
4. J. Wang, M. Maiorov, D.S. Baer, D.Z. Garbuzov, J.C. Connolly, R.K. Hanson: Appl. Opt. **39**, 5579 (2000)
5. L.S. Rothman, C.P. Rinsland, A. Goldman, S.T. Massie, D.P. Edwards, J.M. Flaud, A. Perrin, C. Camy-Peyret, V. Dana, J.Y. Mandin, J. Schroeder, A. McCann, R.R. Gamache, R.B. Wattson, K. Yoshino, K.V. Cance, K.W. Jucks, L.R. Brown, V. Nemtchinov, P. Varanasi: J. Quant. Spectrosc. Radiat. Transfer **60**, 665 (1998)
6. D. Weidmann, D. Courtois: Infrared Phys. Technol. **41**, 361 (2000)
7. M. Tacke, B. Spanger, A. Lambrecht, P.R. Norton, H. Böttner: Appl. Phys. Lett. **53**, 2260 (1988)
8. M. Othsu, Y. Teramachi: IEEE J. Quantum Electron. **QE-25**, 31 (1989)
9. R.M. Fristrom, A.A. Westenberg: *Flame Structure* (McGraw-Hill, New York 1965)
10. A.G. Gaydon, H.G. Wolfhard: *Flames* (Chapman and Hall, London 1970)
11. M.R. DeBacker, B. Parvitte, X. Thomas, V. Zeninari, D. Courtois: J. Quant. Spectrosc. Radiat. Transfer **59**, 3 (1998)
12. D. Bradley, J. Matthews: J. Mech. Eng. Sci. **10**, 299 (1968)
13. J.J. Olivero, R.L. Longbothum: J. Quant. Spectrosc. Radiat. Transfer **17**, 233 (1977)
14. A. Hamdouni, A. Barbe, P. Demoulin, R. Zander: J. Quant. Spectrosc. Radiat. Transfer **57**, 11 (1997)
15. C. Boussin, B.L. Lutz, A. Hamdouni, C. De Bergh: J. Quant. Spectrosc. Radiat. Transfer **63**, 49 (1999)